reasonably be expected to produce reliable results for the S waves.

*Work supported in part by the U. S. Atomic Energy Commission.

[1]A. E. Everett, Phys. Rev. 173, 1663 (1968).
[2]L. A. P. Balázs, Phys. Rev. 137, B1510 (1965).
[3]J. Finkelstein, Phys. Rev. 145, 1185 (1966).
[4]R. Capps, Phys. Rev. 131, 1307 (1963); S. Gasiorowicz, *Elementary Particle Physics* (Wiley, New York, 1966), pp. 325–326.
[5]J. J. de Swart, Rev. Mod. Phys. 35, 916 (1963).
[6]B. Oh, A. Garfinkel, R. Morse, W. Walker, J. Prentice, E. West, and T. Yoon, Phys. Rev. D 1, 2494 (1970).
[7]Particle Data Group, Rev. Mod. Phys. 43, S1 (1971).
[8]A. Ahmadzadeh, P. Burke, and C. Tate, Phys. Rev. 131, 1315 (1963).
[9]U. Trivedi, Phys. Rev. 188, 2241 (1969).
[10]P. Carruthers and M. Nieto, Phys. Rev. 163, 1646 (1967); E. Golowich, *ibid.* 158, 1745 (1968); S. Mandelstam, *Elementary Particle Physics* (Benjamin, New York, 1967), Part II, p. 1.
[11]Y. Cho *et al.*, Phys. Letters 32B, 409 (1970); A. M. Bakker *et al.*, Nucl. Phys. B24, 211 (1970).
[12]A. E. Everett, Phys. Rev. D 4, 2797 (1971).
[13]H. Yuta *et al.*, Phys. Rev. Letters 26, 1502 (1971).
[14]S. Weinberg, Phys. Rev. Letters 17, 616 (1966); R. W. Griffith, Phys. Rev. 176, 1705 (1966).

PHYSICAL REVIEW D VOLUME 5, NUMBER 7 1 APRIL 1972

Quantitative Regge Expressions with Scaling for Experimentally Measured Fast $\pi^{\pm}, K^{+}$ Inclusive Spectra and Relation to Backward-Elastic-Scattering Data*

Clifford Risk†
Lawrence Radiation Laboratory, University of California, Berkeley, California 94721
and Department of Physics, University of California, Davis, California 95616
(Received 30 June 1971)

We represent the spectra for fast π^+, π^-, K^+ secondaries in pp collisions in Reggeized forms that describe the experimental data measured at several energies and that scale at high energies. We relate the inclusive amplitudes obtained to backward elastic $\pi^{\pm}p, K^+p$ scattering and predict both their relative magnitudes and their energy and angle dependence.

I. INTRODUCTION

The inclusive reaction $p+p \to X+$anything, where X is a specified secondary, offers the simplest probe of the dynamics of particle production processes, and has recently been the subject of experimental and theoretical study. Particle spectra have been measured in pp collisions at momenta of 12.4 GeV/c,[1] 19.2 GeV/c,[2] and 30 GeV/c.[3] General considerations about the features of the spectra have been proposed by Feynman[4] and Benecke, Chou, Yang, and Yen[5]; Vander Velde[6] has demonstrated the equivalence of their approaches and shown that the fast secondaries of Refs. 1–3 satisfy their predictions. Calculations of the spectra within specific models – the multi-Regge model[7–9] and the Hagedorn thermodynamic model[10] – have been compared with the measured data.

In this paper we show that the spectra of fast produced $\pi^{\pm}$, K^+ in pp collisions can be represented by Reggeized expressions that scale at large energy, and that such expressions are intrinsically related to the experimental backward $\pi^{\pm}p$ and K^+p elastic two-body differential cross sections. This approach will allow us not only to predict the inclusive fast spectra at high energies, but also to extract the properties of backward elastic cross sections at lower energies.

Consider first the process $p+p \to m+$anything of Fig. 1(a), with "m" a produced meson and M^2 representing the remaining secondaries. We will describe those produced $\pi^{\pm}, K^+$ that emerge with large momentum in the center-of-mass (c.m.) system, and hence with large positive momentum or small negative momentum in the lab. In a multi-Regge model, these mesons emerge at the end of the multiperipheral chain, with the incident proton traveling a link down the chain and peripherally scattering with the other incident proton [Fig. 1(b)]. We represent this process with the diagram of Fig. 1(c), the cross section of which is

$$\frac{d^2\sigma}{dt\,dM^2} = \frac{1}{s^2}\left(\frac{s}{M^2}\right)^{2\alpha(t)} \beta^2(t) M^2 \sigma_T(M^2) . \qquad (1)$$

Here, $\alpha(t)$ is the effective trajectory of the exchanged baryon, $\beta(t)$ is its residue, and $\sigma_T(M^2)$ is the total cross section for the baryon-baryon scattering. Such an expression was first obtained by Caneschi and Pignotti[7] several years ago on the basis of multi-Regge theory. Recently, Peccei and Pignotti[11] have further studied the experimental consequences of (1).

We organize the paper as follows. In Sec. II we discuss the spectra predicted by (1), and its approach to a scaling limit. In Sec. III we obtain quantitative expressions of the type (1) for the $\pi^{\pm}, K^{+}$ spectra from the 19.2-GeV/c data. In Sec. IV we test the scaling predictions of (1) by comparing with the 12.4-GeV/c and 30-GeV/c data. The shape of the fast backward spectra predicted by (1) should be independent of the incident particle, and in Sec. V we compare (1) with the π^{-} fragmentation of the proton in $K^{+}p$ collisions at 12.4 GeV/c. In Sec. VI we discuss the relation between the inclusive inelastic process of (1) and the elastic backward meson-proton differential cross sections, and we use this relation to predict energy dependence, angle dependence, and relative normalization of the three processes. Section VII contains remarks about the K^{-}, $\bar{p}$, and p spectra.

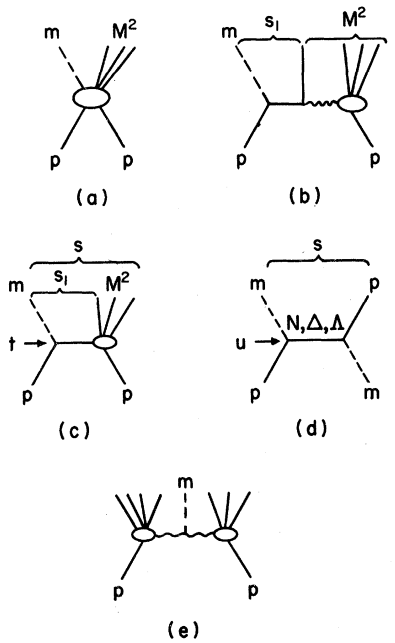

FIG. 1. (a)–(e) Diagrams for fast mesons; m,p refer to meson and proton, respectively; M^2, s, s' refer to invariant energies squared. (a) Diagram for a produced meson. (b) Multi-Regge representation of (a) for a fast meson. (c) Multi-Regge diagram used in this paper. (d) Diagram for backward elastic meson-proton scattering. (e) Meson produced internally in the multi-Regge model.

II. SPECTRUM PREDICTED BY EQ. (1)

The momentum spectrum predicted by (1) will be given by

$$d^3\sigma = \frac{d^3p}{E}\frac{2mp_0}{\pi}\frac{d^2\sigma}{dtdM^2}\,. \tag{2}$$

Here, p and E are the momentum and energy of the secondary, p_0 is the incident beam momentum. We can express (2) in terms of the longitudinal- and transverse-momentum components p_L, p_T of the secondary in the c.m. system by using

$$t = m^2 + \mu^2 + 2(\bar{p}_0 p_L - \bar{E}_0 E)\,, \tag{3a}$$

$$M^2 = 4\bar{E}_0^{\,2} - 4\bar{E}_0 E + \mu^2\,. \tag{3b}$$

μ is the mass of the secondary, and $\bar{p}_0, \bar{E}_0$ are the c.m. momentum and energy of the incident particle. When p_L and $\bar{p}_0$ are both large, we introduce $x = p_L/\bar{p}_0 \sim E/\bar{E}_0$, and t, M^2 become

$$t = m^2(1-x) + \mu^2 - (p_T^{\,2} + \mu^2)/x\,, \tag{4a}$$

$$M^2 = s(1-x)\,. \tag{4b}$$

The spectrum is then given by

$$d^3\sigma = \frac{d^3p}{E}\frac{(1-x)^{1-2\alpha(t)}}{\pi}\beta^2(t) \tag{4c}$$

$$= \frac{d^3p}{E} f(x, p_T)\,, \tag{4d}$$

where $f(x, p_T)$ is the Feynman scaling function.

In the lab system, the expressions for t, M^2 become

$$t = m^2 + \mu^2 - 2(p_0 p_L - E_0 E) \rightarrow m^2(1-R) + \mu^2 - (p_T^{\,2} + \mu^2)/R\,, \tag{5a}$$

$$M^2 = (E_0 + m - E)^2 - p_0^{\,2} - p^2 + 2p_0 p_L \rightarrow s(1-R)\,, \tag{5b}$$

where $R = p/p_0 \approx p_L/p_0$, as introduced by Vander Velde,[6] and the spectrum becomes

$$d^3\sigma = \frac{d^3p}{E} f(R, p_T)\,. \tag{5c}$$

Finally, we can derive the expression for slow secondaries in the lab (backward fast secondaries in the c.m. system) by writing t, M^2 relative to the target:

$$t = m^2 + \mu^2 - 2mE\,, \tag{6a}$$

$$M^2 = (E_0 + m - E)^2 - p_0^{\,2} - p^2 + 2p_0 p_L \rightarrow s[1 - (E - p_L)/m]\,, \tag{6b}$$

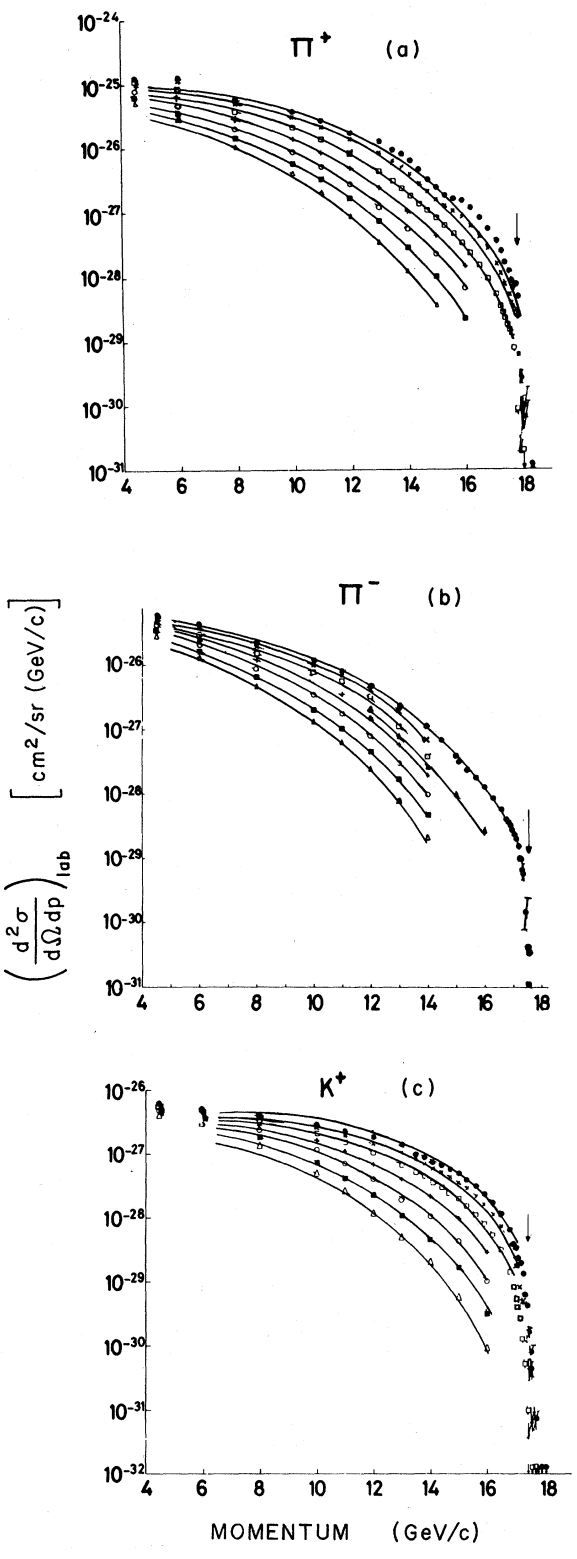

FIG. 2. (a)–(c) Spectra for fast $\pi^{\pm}$, K in pp collisions at 19.2 GeV/c. The solid lines are the theoretical representation of the data obtained in this paper.

$$d^3\sigma = \frac{d^3p}{E}\frac{1}{\pi}\left(1-\frac{E-p_L}{m}\right)^{1-2\alpha(t)}\beta^2(t). \tag{6c}$$

Equation (6c) depends only on p_L, p_T and is independent of p_0, as conjectured by Benecke *et al.*[5] and Vander Velde.[6]

III. QUANTITATIVE EXPRESSIONS FOR THE SPECTRA

To derive quantitative expressions for the secondary spectra, first we compare Eq. (1) with the 19.2-GeV/c data (Fig. 2). We cut the data at fixed M^2 (Fig. 3) and plot against t. This gives Figs. 4(a)–4(c). Perhaps the most interesting features of the data are the sharp forward t dependence and the shrinking diffraction behavior as M^2 decreases (or the Regge subenergy s/M^2 increases).

If Eq. (1) is to represent the data, then a plot of the cross section at fixed t against M^2 on a log-log graph should give straight lines of slope $2\alpha(t)-1$. These plots are shown in Figs. 5(a)–5(c). The π^+ cross section in Fig. 5(a) shows the most dramatic Regge behavior, with straight lines over as much as $2\frac{1}{2}$ decades in the data. The π^- and K^+ data also show Regge behavior over $M^2 < 20$ GeV^2.

The Regge trajectories $\alpha(t)$ can now be evaluated from the slopes of Fig. 5 (we take $\sigma_T \equiv 1$), and they are graphed in Fig. 6. The relatively low intercepts are at first surprising, but we shall see that this corresponds to the relatively fast fall in the backward elastic processes in the intermediate-energy range ($p_0 = 2$–4 GeV/c).

Next we assume the cross section does take the

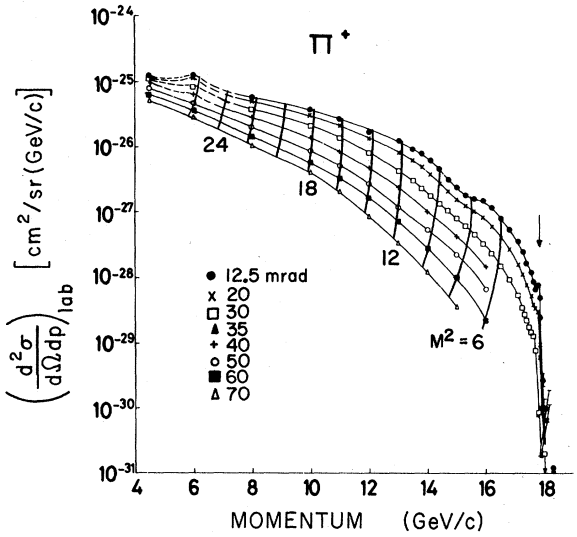

FIG. 3. Cuts on the data of Fig. 2(a) at fixed M^2. The curved lines are from Ref. 1.

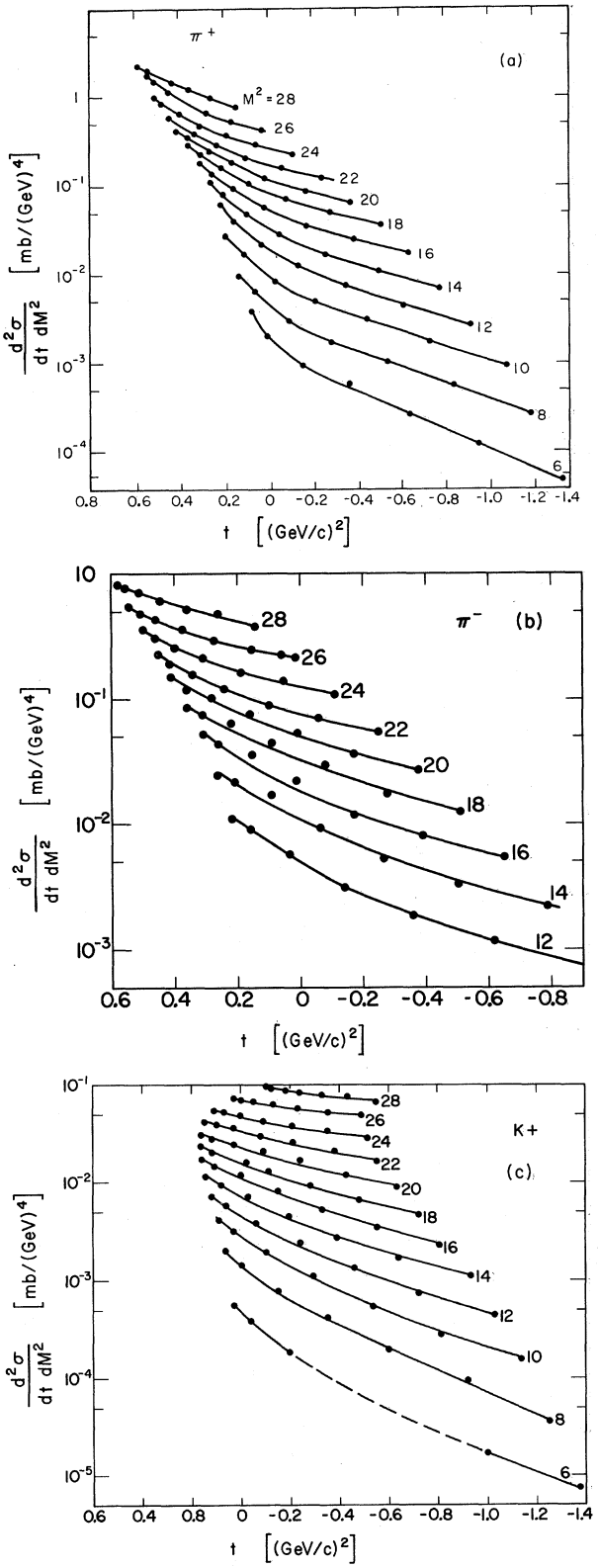

FIG. 4. (a)–(c) The data of Fig. 2 replotted at fixed M^2 against t. Dots represent the interpolations of the data of Fig. 2 and Fig. 3.

form (1) and set $s = 37.8$ GeV^2 – the s dependence will be verified by comparing (1) with spectra at other energies. We solve for the residues $\beta^2(t)$, and this gives Fig. 7.

Collecting these results, we compare (2) with the experimental data in Fig. 2.

1. π^+ spectra. Equation (2) adequately represents the data for $R > 0.4$, except for the structure at $p = 14$ GeV/c. For $R < 0.4$, we expect the diagram of Fig. 2(e) (internal pionization) to contribute to the spectrum, and Eq. (2) falls below the data.

2. π^- spectra. Equation (2) represents the data for $R > 0.4$. Note that the π^- spectrum at 12.5 mrad falls by 3 decades from $p = 4.5$ GeV/c to $p = 16$ GeV/c, while the π^+ spectrum falls only 2 decades. It is this relatively rapid falloff in the fast π^- spectrum in the Regge region that leads to the low value of $\alpha_\Delta(t)$, and this is related to the relatively rapid falloff in the $\pi^- p$ backward elastic cross section (Sec. VI).

3. K^+ spectra. Equation (2) represents the data for $R > 0.5$, except for the 12.5-mrad data, which gives a p_T dependence at $p_T \sim 0$ that becomes very broad for $p < 12$ GeV/c. Generally, the momentum dependence of K^+ spectra is similar to that of the π^+, and this leads to the similarity of their trajectories in Fig. 6.

In all cases, Eq. (2) overestimates the data for $R \gtrsim 0.98$ as p approaches the kinematical limit at $p \sim 19$ GeV/c, because the condition that $\sigma_T(M^2) \to 0$ at threshold has not been used.

IV. COMPARISON WITH 12.4-GeV/c AND 30-GeV/c DATA

The trajectories and residues of Figs. 6 and 7 have been obtained from Eq. (2) by fixing $s = 37.8$ GeV^2. To test the energy dependence of (2), we compare our quantitative expressions with the data at 12.4 GeV/c and 30 GeV/c in Fig. 8.

1. π^+ data [Fig. 8(a)]. The data at $p_T^2 = 0.22$ (GeV/c)^2 are adequately predicted for $x > 0.4$. The data at $p_T^2 = 0.43$ (GeV/c)^2 stops at somewhat small x for a comparison. In Fig. 8(c), the prediction at 15 mrad is adequate for $R > 0.2$.

The dashed lines in Figs. 8(a) and 8(c) represent extrapolations of Fig. 6 to the range of $t < -1.2$ GeV^2, where Ref. 1 had no data. These extrapolations were obtained by linearity extending $\alpha(t)$ and taking $\beta_N^2(t)$ as listed in Table I. Other extrapolations – such as a flattening $\alpha(t)$ – could have been used; there are too few data for a unique extrapolation and we report our result only as a guide.

2. π^- data. The features of the π^- predictions Figs. 8(b) and 8(c) are similar to those of the π^+, except that at both energies they are on the aver-

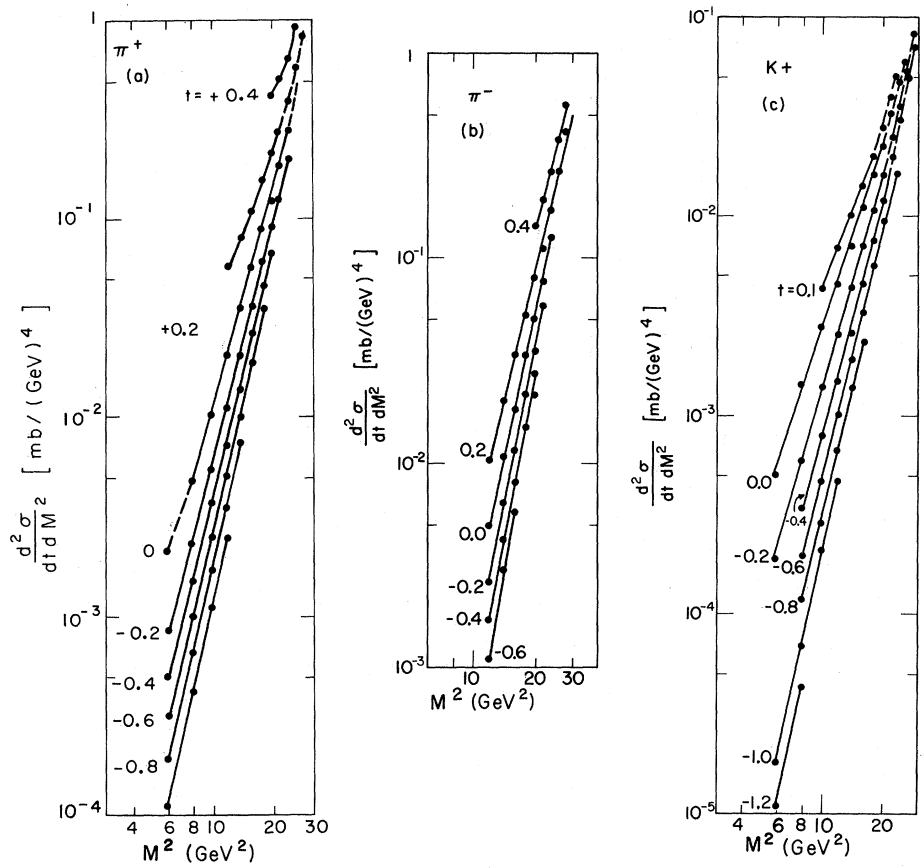

FIG. 5. (a)–(c) The data of Fig. 4 replotted at fixed t against M^2.

age 50% above the data. This result was also obtained by Vander Velde[6] in his scaling analysis of the data and represents possible differences in the over-all normalization of the different experiments. In counter experiments, such discrepancies are possible.[12]

V. COMPARISON WITH π^- FROM Kp DATA

The spectra of the fast π^- that are backward in the c.m. system should be the same in Kp collisions as in pp collisions. In the multiperipheral model this comes about from these π^- being

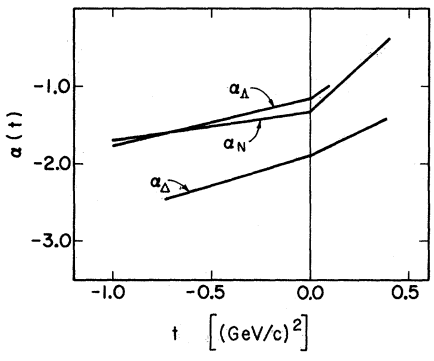

FIG. 6. Effective trajectories obtained from the slopes of Fig. 5; α_N, α_Δ, α_Λ refer to the trajectories for the π^+, π^-, and K spectra, respectively.

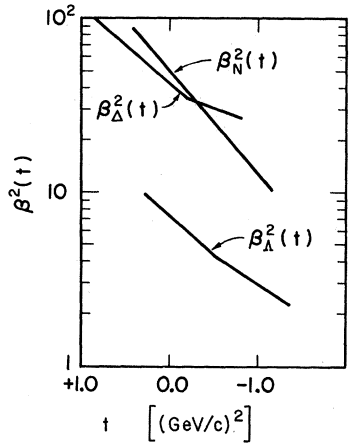

FIG. 7. Residues $\beta^2(t)$ obtained from Figs. 4 and 6.

emitted at the proton end of the chain and hence having a spectrum independent of the beam particle. To test the present model with this conjecture, we compare the prediction of (2) with the spectrum of Ko and Lander[13] in Fig. 9. The agreement is reasonable. In particular, note that Eq. (2) describes the π^- mesons with small p_T to a small value of x, $x \sim 0.2$, but π^- mesons with large p_T only up to $x \sim 0.5$. As discussed in Ref. 9, this occurs because Figs. 1(b) and 1(c) give rise to the forward-scattered mesons at small p_T, whereas Fig. 1(e) gives rise to mesons at larger values of p_T. Hence the extrapolation of Eq. (2) to small x when p_T is small is expected to be good.

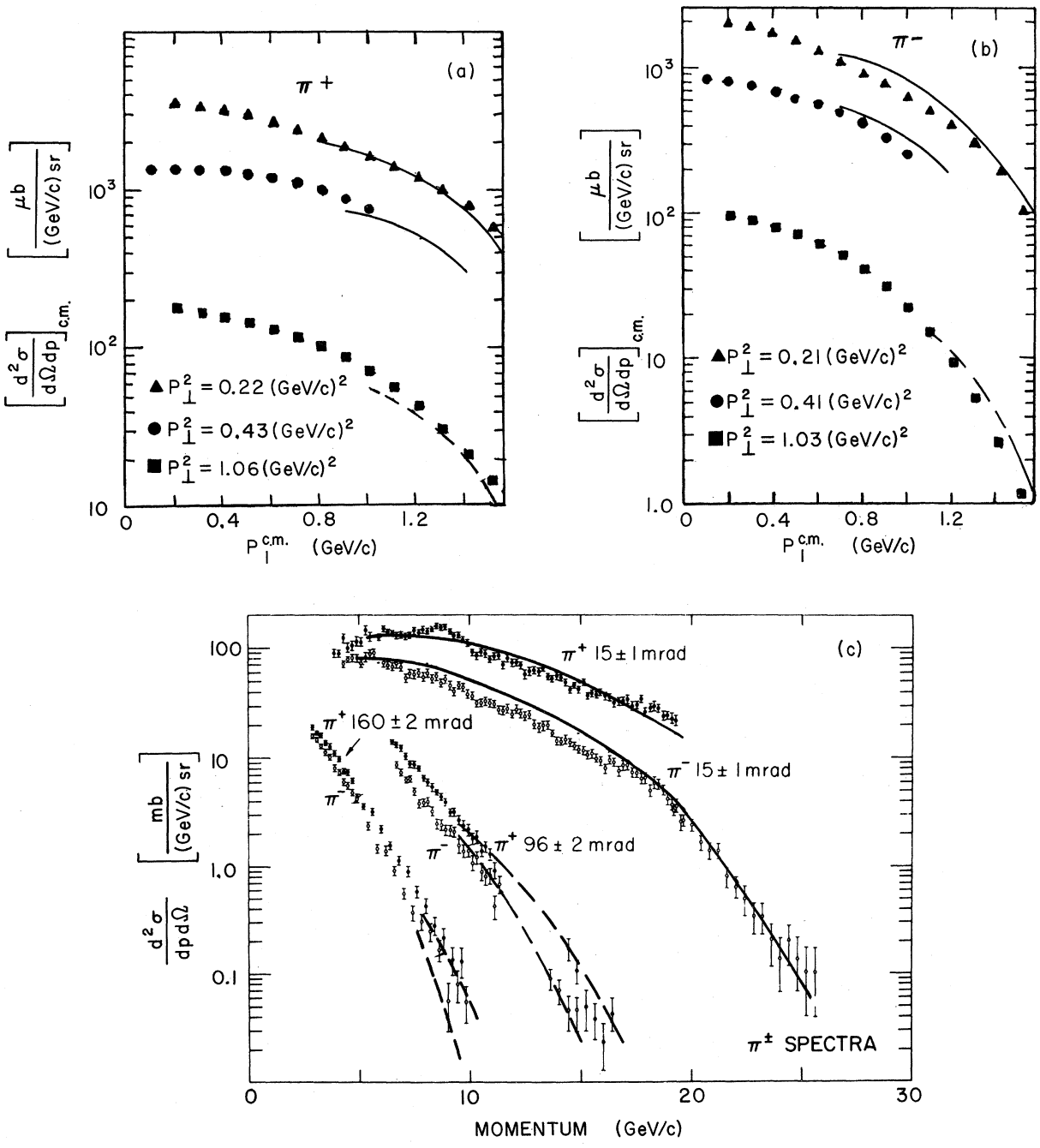

FIG. 8. Predictions of Eq. (2) for the $\pi^{\pm}$ data: (a) and (b) at 12.4 GeV/c; and (c) at 30 GeV/c.

VI. RELATION OF INCLUSIVE SPECTRA TO TWO-BODY ELASTIC BACKWARD CROSS SECTIONS

The multiperipheral diagrams of Fig. 1 impose a direct relation between the inclusive inelastic process and the elastic backward process. If we neglect the off-mass-shell effects of the exchanged baryon in Fig. 1(b), then we are led to represent the two-body process of Fig. 1(d) as

$$\frac{d\sigma(s,u)}{du} = \frac{c}{s^2} s^{2\alpha(u)} \beta^2(u), \tag{8}$$

where c is a constant. That is, we expect generally that if the two-body process is represented by

$$\frac{d\sigma(s,u)}{du} = \frac{c}{s^2} |A(s,u)|^2, \tag{9a}$$

then the inclusive process is given by

$$\frac{d^2\sigma(s,t,M^2)}{dt\,dM^2} = \frac{1}{s^2} |A(s/M^2, t)|^2 M^2 \sigma_T(M^2). \tag{9b}$$

In writing Eqs. (9a) and (9b), we have made a number of assumptions which we discuss below.

Over what energy range should we expect to predict the two-body data? In the Allaby data, $s = 37.8$ GeV^2, and the representations obtained have adequately described the inclusive data for $M^2 = 6$–20 GeV^2. Therefore, we are led to predict the two-body data with Eq. (8) for $s \sim 2$–8 GeV^2; this corresponds to the intermediate-energy range extending from just above the $\Delta(1236)$ resonance region to the onset of the high-energy pure Regge region.

To test this relation, we have evaluated Eq. (8) for the three backward elastic processes: $\pi^+ p$, $\pi^- p$, $K^+ p$. In this comparison, we normalize one process ($\pi^- p$) to the data and then predict the normalizations of the remaining two processes and the s and u dependence of all three.

In Figs. 10(a)–10(c) we compare the predicted backward elastic cross section at 180° with the experimental data[14–17] as a function of energy. In Fig. 10(a), the π^+ prediction represents an average of the backward two-body behavior. The ab-

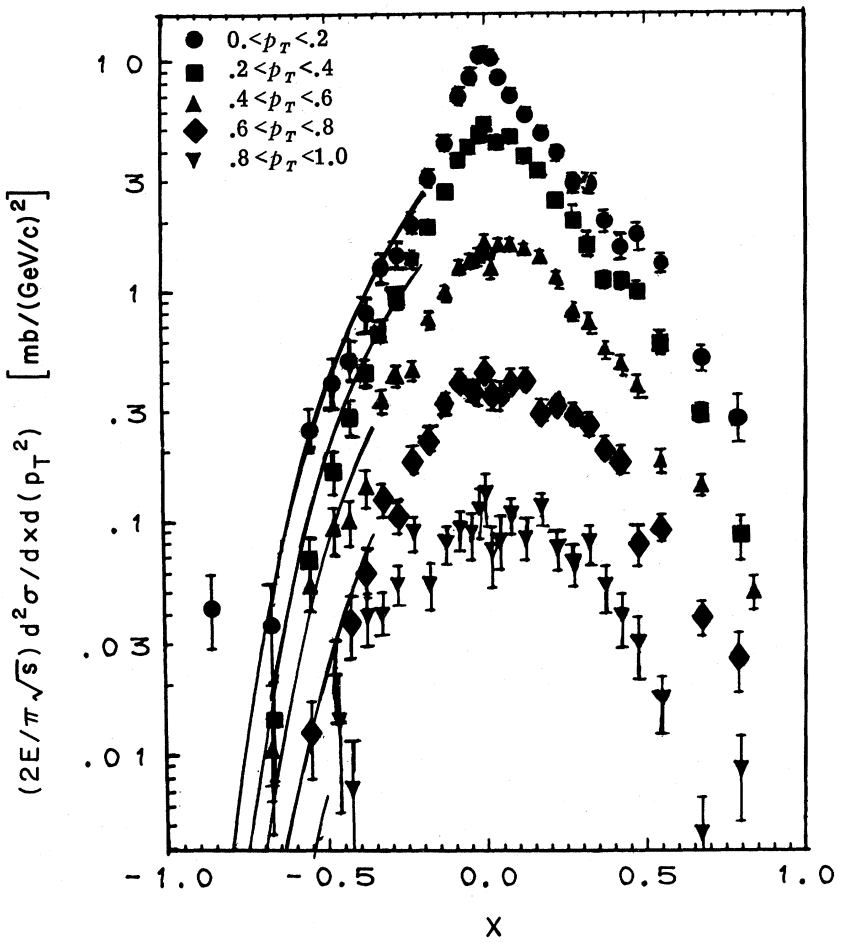

FIG. 9. Predictions of Eq. (2) for the π^- data from $K^+ p$ collisions at 11.8 GeV/c. To account for the known p_T distribution in each bin, the theoretical curves are calculated at $p_T = 0.13$, 0.3, 0.48, 0.68, 0.88 GeV/c.

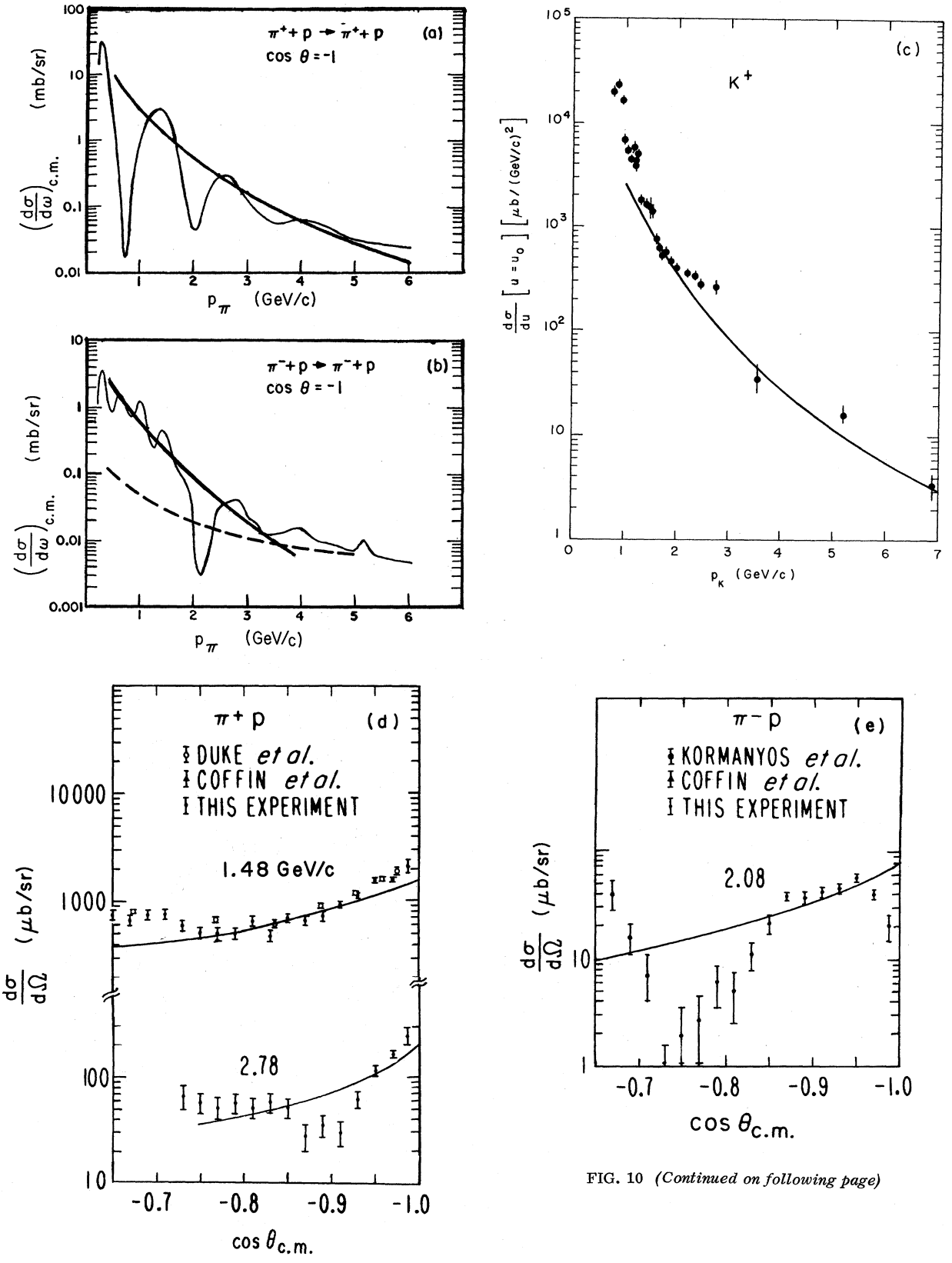

FIG. 10 *(Continued on following page)*

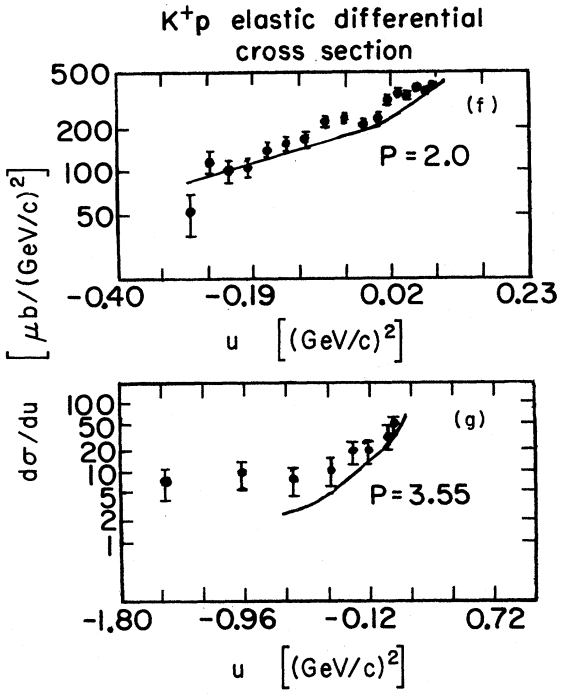

FIG. 10. Predictions of Eq. (8) for backward π^+p, π^-p, K^+p elastic differential cross sections. (a) and (c) Momentum dependence at 180°. (d)–(g) Angle dependence at fixed momentum. In Fig. 10(b), the dashed line is the duality prediction of Ref. 18.

TABLE I. Parameters representing the data.[a]

$\alpha_N(t)$	$=-1.35+1.25t$,	$t>0$
	$=-1.35+0.35t$,	$t<0$.
$\alpha_\Delta(t)$	$=-1.9+1.25t$,	$t>0$
	$=-1.9+0.75t$,	$t<0$.
$\alpha_\Lambda(t)$	$=-1.15+1.5t$,	$t>0$
	$=-1.15+0.75t$,	$-0.4<t<0$
	$=-1.25+0.5t$,	$t<-0.4$.
$\beta_N^2(t)$	$=50e^{1.3t}$,	$t>-1.2$
	$=10.5e^{0.345(t+1.2)}$,	$-4<t<-1.2$
	$=4$,	$t<-4$.
$\beta_\Delta^2(t)$	$=35e^{1.03(t+0.2)}$,	$t>-0.2$
	$=35e^{0.47(t+0.2)}$,	$-1<t<-0.2$
	$=35e^{-0.38}$,	$t<-1$.
$\beta_\Lambda^2(t)$	$=7.4e^{1.05t}$,	$t>-0.5$
	$=4.39e^{0.69(t+0.5)}$,	$t<-0.5$.

[a]The $\beta_\Delta^2(t)$ is based on the 19.2-GeV/c data. We recommend an extra factor, $f=\frac{2}{3}$, to bring agreement with the 12.4- and 30-GeV/c data. The constant c in Eq. (8) is 30.

sence of the N^* resonances at 1525, 1670, 1688, and 1700 GeV forces the π^+p cross section to a low average value in the range $p_\pi \sim 1$–2 GeV/c; its average value is one to two times larger than the π^-p cross section. At larger p_π, $p_\pi \sim 4$–5 GeV/c, the π^+p process is 10 times larger than the π^-p process. As discussed in Ref. 9, it is this relatively faster falloff in the π^-p process that leads to the low position of the α_Δ in Fig. 7. [At large p_π beyond the resonance region, $p_\pi > 4$ GeV/c, the canonical trajectories dominate the π^-p cross section and Eq. (8) undercuts the data.] Similarly, for $p_K > 1.5$ GeV/c, the backward K^+p process has an energy dependence similar to the π^+p; this leads to the inclusive π^+, K^+ spectra having similar momentum dependence (Fig. 2) and hence similar trajectories (Fig. 7).

If we now turn to small values of p_π in Fig. 10(a), $p_\pi \sim 1$ GeV/c, we see that the theoretical $d\sigma/d\omega$ undercuts the structure at the $\Delta(1236)$ resonance. This corresponds in Fig. 2(a) to the bump in the π^+ spectrum at $p \sim 6$ GeV/c, which similarly lies above the background predicted by the theoretical distribution. [In Fig. 8(c) this bump occurs at the scaled value $p \sim 9$ GeV/c.] A similar undercutting in the K^+ data in the resonance region occurs in Figs. 2(c) and 10(c).

We can also compare the angular dependence predicted with the experimental data. In Fig. 10(d) we see that the π^+p differential cross section predicted by Eq. (8) is in reasonable agreement with the data. The prediction for the π^-p data in Fig. 10(e) represents an average to the experimentally measured cross section. In Figs. 10(f) and 10(g) there is a reasonable agreement for the K^+p data.

Having seen what a simple application of Eqs. (9a) and (9b) leads to, we return to these equations and discuss the assumptions they involve in more detail.

(1) We have represented the meson-proton two-body interactions of Figs. 1(b) and 1(d) by the exchange of an effective Reggeon. This "Reggeon" is, of course, not a bona fide canonical Reggeon, but simply a duality representation of all the complicated baryon resonances that dominate these amplitudes. What has been most surprising is that the trajectories in Fig. 6 obtained from the inclusive data then predict the energy dependence of the elastic backward amplitudes so well. In Fig. 10(b), the dashed line indicates the duality extrapolation obtained by Barger and Cline[18] using the conventional Regge poles. We see that the inclusive process provides a more sensitive probe of the two-body process in this energy region.

(2) The exchanged Reggeon will be off-mass-shell, and so the total cross section σ_T for the Reggeon-target interaction will have a t dependence. We have assumed that this term is given by the

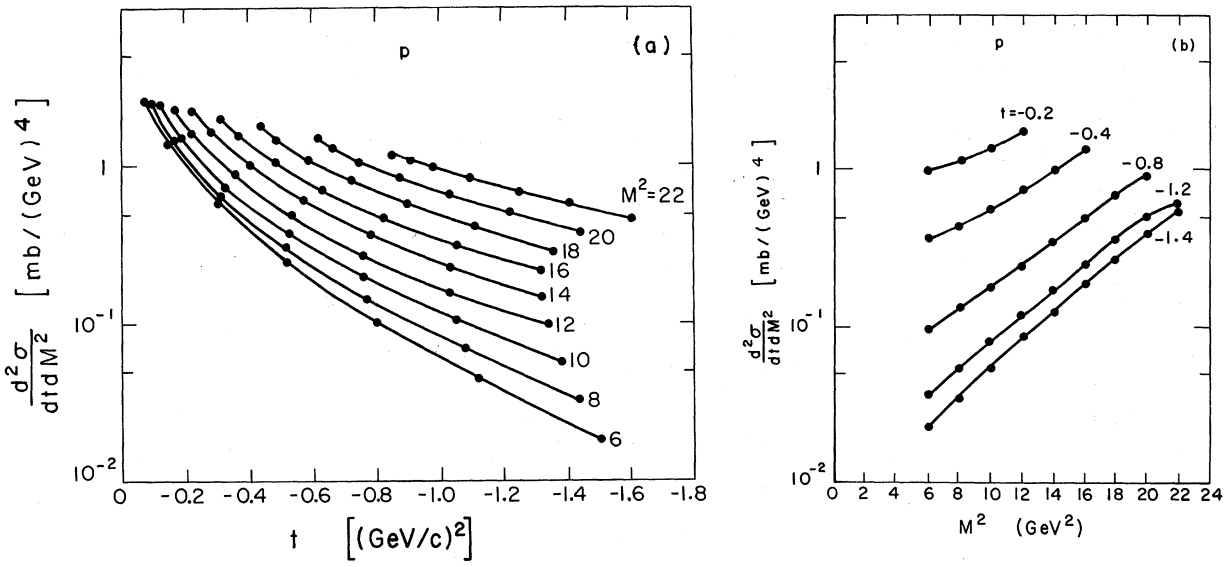

FIG. 11. The proton spectra at 19.2 GeV/c. Plotted (a) at fixed M^2 against t; (b) at fixed t against M^2.

residue term already incorporated into the elastic amplitude $A(s, t)$, and hence is contained in $A(s/M^2, t)$. Comparing Figs. 10(d)–10(g), we see that in an average sense this approximation is reasonably good.

(3) We have assumed that the total cross sections $\sigma_T(M^2)$ are all equal to unity for the three processes considered. This is perhaps the strongest assumption, because it has led us to predict the relative rates for the two-body processes from those for the inclusive processes.

VII. THE K^-, $\bar{p}$, AND p SPECTRA

The spectra for K^-, $\bar{p}$, and p secondaries are very different from the $\pi^\pm, K^+$ secondaries. We expect few fast K^-, because the backward K^-p elastic cross section falls very rapidly in the intermediate energy range. An analysis of the type performed here should lead to a low effective trajectory, with an intercept ~ -4.

Similarly, we expect no fast $\bar{p}$ at all because of the absence of double-baryon exchange in Fig. 1(c).

The proton spectrum is a special case. If we plot the data at fixed M^2 against t, we obtain Fig. 11(a), we again obtain sharp forward peaking at small t; but in contrast to the $\pi^\pm, K^+$ spectra, there is no shrinking diffraction peak. This can be seen in Fig. 11(b), where we plot the data at fixed t against M^2 on a *log* plot. The indication of straight lines suggests a representation of the form

$$\frac{d^2\sigma}{dt\,dM^2} \sim \frac{e^{a(t)M^2/s}}{s}\,\beta^2(t). \tag{10}$$

By performing this analysis on the data at the other two energies of Refs. 2 and 3, we have found that the exponent of Eq. (10) does take the scaling form indicated.[19] These results will be reported elsewhere.

ACKNOWLEDGMENTS

I am very grateful to Professor Richard Lander for the hospitality extended to me at Davis during the present year. I am also grateful to Professor Lander and Dr. Winston Ko for fruitful discussions leading to completion of the work, and to members at Davis of the Physics 129 seminar for stimulating interactions. Discussions with Professor J. Ball, Dr. W. Swanson, Professor L. Stevenson, and Professor V. Chung are appreciated. Professor G. Chew and Professor J. D. Jackson are warmly thanked for the hospitality of Lawrence Radiation Laboratory.

The present work has greatly benefited from a collaboration with Dr. J. H. Friedman involving development of phenomenological models for inelastic processes.

*Work supported in part under the auspices of the U. S. Atomic Energy Commission.

†Participating guest at Lawrence Radiation Laboratory, Berkeley, Calif.

[1]C. W. Akerlof *et al.*, Phys. Rev. D 3, 645 (1971).
[2]J. V. Allaby *et al.*, CERN Report No. CERN-TH-70-12, 1970 (unpublished).
[3]E. W. Anderson *et al.*, Phys. Rev. Letters 19, 198 (1967).
[4]R. P. Feynman, in *High Energy Collisions*, Third International Conference held at State University of New York, Stony Brook, 1969, edited by C. N. Yang, J. A. Cole, M. Good, R. Hwa, and J. Lee-Franzini (Gordon and Breach, New York, 1969).
[5]J. Benecke, T. T. Chou, C. N. Yang, and E. Yen, Phys. Rev. 188, 2159 (1969).
[6]J. C. Vander Velde, Phys. Letters 32B, 501 (1970).
[7]L. Caneschi and A. Pignotti, Phys. Rev. Letters 22, 1219 (1969).
[8]L. Caneschi, D. E. Lyon, Jr., and Clifford Risk, Phys. Rev. Letters 25, 774 (1970).
[9]Clifford Risk and Jerome H. Friedman, Phys. Rev. Letters 27, 353 (1971).
[10]J. Ranft, Phys. Letters 33B, 481 (1970).
[11]R. D. Peccei and A. Pignotti, Phys. Rev. Letters 26, 1076 (1971).
[12]J. Vander Velde and D. Smith (private communications).
[13]W. Ko and R. Lander, Phys. Rev. Letters 26, 1064 (1971); 26, 1284 (1971).
[14]The experimental data of Fig. 10 have been taken from the following: Figs. 10(a) and 10(b) from Ref. 15; Fig. 10(c) from tabulation of Ref. 16; Figs. 10(d) and 10(e) from Ref. 17; Fig. 10(f) from Ref. 16.
[15]H. L. Anderson *et al.*, Phys. Rev. D 3, 1536 (1971).
[16]Particle Data Group, LRL Report No. UCRL-20000 K^+N, 1969 (unpublished).
[17]A. S. Carroll *et al.*, Phys. Rev. Letters 20, 607 (1968).
[18]V. D. Barger and D. B. Cline, Phys. Letters 27B, 312 (1968).
[19]The form of Eq. (10) arises from the contribution to the proton spectrum from Fig. 1(b) (J. Ball, private communication). These protons have become inelastic and are scattered into larger angles. In Ref. 9, this portion of the spectrum was described by the sum of the contribution from Fig. 1(b) and the diagram for the fast proton emerging at the end of the multi-Regge chain.

PHYSICAL REVIEW D VOLUME 5, NUMBER 7 1 APRIL 1972

Pion-Nucleon *P*-Wave Scattering Amplitudes and Their *S*-Matrix Calculations

V. F. Šachl
Department of Mathematics, University of Durham, Durham, England
*and Institute of Physics, Czechoslovak Academy of Sciences, Prague, Czechoslovakia**
(Received 25 June 1971)

The effective-range formulas for the P-wave scattering amplitudes, $I=\frac{1}{2}$ and $I=\frac{3}{2}$, of pions on nucleons are derived for the low-energy region using the requirements of analyticity, unitarity, and crossing symmetry and a sum rule. The S-matrix calculations are carried out by the generalized one-channel Chew-Mandelstam method in which the denominator function D may, generally, contain a Castillejo-Dalitz-Dyson (CDD) pole, while the function N is considered in the three-pole effective-range approximation. The effective-range parameters are then determined by the usual procedure in which the input values are the ρ-meson and (3,3)-isobar N^* discontinuities and the high-energy contributions in the crossed channels, and the nucleon pole in the direct channel. The amplitudes P_{13} and P_{33}, derived in this way as functions of the CDD-pole term, are then compared with experiment by means of the calculated and experimental values of the scattering lengths a_{13} and a_{33}. It is shown, as one of the main results, that the low-energy P_{13} amplitude does not contain any CDD pole and produces a scattering length which is in excellent agreement with the experimental value, while the P_{33} amplitude necessarily contains a nonzero pole term. These results are in agreement with the conclusions made on the basis of a quite different approach – the "crankshaft analysis" – in the papers by Atkinson *et al.*

I. INTRODUCTION

S-matrix calculations enable us generally to derive analytically the partial-wave scattering amplitudes in strong interactions, which are consistent with the requirements of analyticity, unitarity, and crossing symmetry.

An approximative approach which starts from these requirements and determines the partial-wave amplitudes in a certain low-energy region has been worked out as the N/D effective-range method by Balázs.[1]

The determining left-hand cut in the s-plane is replaced in this approximation by several (in our case two) poles s_i so that the numerator function N is given as a sum of n fractions $b_i/(s-s_i)$ with unknown residues b_i.

To solve the problem of finding the N/D amplitudes, we determine these residues in our self-consistent calculations by comparison of the